On the Dynamics of Excitation and Information Processing in F-actin: Automaton Model

Andrew Adamatzky
Unconventional Computing Lab, UWE
Bristol BS16 1QY UK

A filamentous actin molecule is represented as a graph of finite-state machines (F-actin automata). Each node in the graph takes three states—resting, excited and refractory. All nodes update their states simultaneously and by the same rule. Two rules are considered: the threshold rule—a resting node excites if it has at least one excited neighbor, and the narrow excitation interval rule—a resting node excites if it has exactly one excited neighbor. The distributions of transient periods and lengths of limit cycles in F-actin automata are analyzed. Mechanisms of limit cycle emergence are proposed and we speculate on how these can be used to store information in a single actin unit. It is demonstrated that OR, AND-NOT and XOR gates can be implemented by excitation dynamics in F-actin automata.

1. Introduction

Actin is a protein present in all eukaryotic cells in the form of globular actin (G-actin) and filamentous actin (F-actin) [1–3]. G-actin polymerizes in the double helix of filamentous actin (Figure 1(a)); during polymerization, G-actin units slightly change their shapes and thus become F-actin units [4]. The actin filaments form a skeleton of single cells, where they play key roles in motility and shape changing—together with myosin, and signal transduction—together with tubulin microtubules [5]. Actin filament networks are key components of neural synapses [6]. The actin network is a substrate of cell-level learning [7–15] and information processing [6, 16–18]. Actin filaments process information in synapses and cells; they compute in a hardwired sense, as specialized processors. If we did manage to uncover the exact mechanisms of information transmission and processing in the actin filaments and establish an interface with actin filaments, we would be able to make large-scale massive-parallel nano-computing devices. In [19] we proposed a model of actin filaments as two chains of one-dimensional binary-state semi-totalistic automaton arrays. We discovered automaton state transition rules that support traveling

https://doi.org/10.25088/ComplexSystems.26.4.295

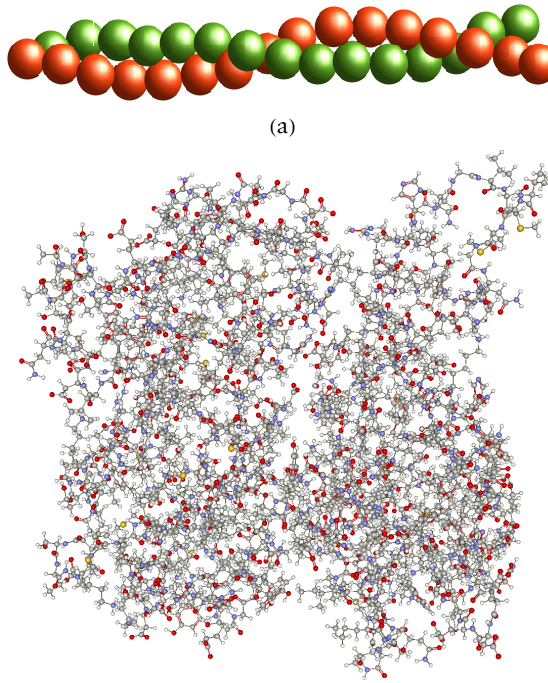

(a)

(b)

Figure 1. Actin structure. (a) Schematic drawing of an actin helix. Spheres are colored for visual guidance only. Each sphere is an F-actin unit, whose molecular structures are shown in (b). (b) F-actin molecule, CPK coloring.

localizations, compact clusters of nonresting states. These traveling localizations are analogous to ionic waves proposed in actin filaments [20]. We speculated that a computation in actin filaments could be implemented when localizations (defects, conformational changes, ionic clouds, solitons), which represent data, collide with each other and change their velocity vectors or states. Parameters of the localizations before a collision are interpreted as values of input variables. Parameters of the localization after the collision are values of output variables. We implemented a range of computing schemes in several families of actin filament models, from quantum automata to lattices with Morse potential [21–25]. These models considered a unit (F-actin) of the filament as a single, discrete entity that can take just two or three states, and carriers of information occupied one to two actin units. These were models of rather coarse-grained computation [21–25]. To take the paradigm of computation via interaction with traveling localizations at the submolecular level, we must understand how information, presented by a perturbation of some part of an

F-actin unit from its resting state, propagates in the F-actin unit, and explore if and how computing devices can be implemented in a single F-actin molecule.

The paper is structured as follows. We define a model of F-actin automata in Section 2. In Section 3 we study the excitation dynamics of automata with a threshold excitation rule, and in Section 4 we look at a rule of narrow excitation interval. Stability of the excitation dynamics is analyzed in Section 5. Implementation of memory in F-actin automata is analyzed in Section 6. Section 7 presents results of our search for logical gates in F-actin automata. Implications of our findings for designs of novel computing devices are discussed in Section 8.

2. Model

We used a structure of an F-actin molecule produced using X-ray fiber diffraction intensities obtained from well-oriented sols of rabbit skeletal muscles [4]. The structure was calculated with resolution 3.3Å in the radial direction and 5.6Å along the axis (Figure 1(b)). The molecular structure was converted to a nondirected graph $\mathcal{A}$, where every node represents an atom and an edge corresponds to a bond between the atoms. The graph $\mathcal{A}$ has 2961 nodes and 3025 edges. The minimum degree is 1, the maximum is 4, the average is 2.044 (with standard deviation 0.8) and the median degree is 2. There are 883 nodes with degree 1, 1009 nodes with degree 2, 1066 nodes with degree 3 and two nodes with degree 4. The graph $\mathcal{A}$ has a diameter (longest shortest path) of 1130 nodes, a mean distance (mean shortest path between any two nodes) of 376 and a median distance of 338.

We study the dynamics of excitation in the actin graph $\mathcal{A}$ using the following models. Each node s of $\mathcal{A}$ takes three states: resting ($\circ$), excited ($\oplus$) and refractory ($\ominus$). Each node s has a neighborhood $u(s)$ that is a set of nodes connected to the node s by edges in $\mathcal{A}$. A resting node $s^t = \circ$ excites depending on a number σ_s^t of its excited neighbors in neighborhood $u(s)$: $\sigma_s^t = \sum_{w \in u(s)} \left\{ w^t = \oplus \right\}$. We consider two excitation rules. In rule $\mathcal{A}_0$, a resting node excites if it has at least one excited neighbor: $\sigma_s^t > 0$. In rule $\mathcal{A}_1$, a resting node excites if it has exactly one excited neighbor: $\sigma_s^t = 1$ (we do not consider rules where $\sigma_s^t > 1$ because excitation there becomes extinct quickly). Transitions from excited state to refractory state and from refractory state to resting state are unconditional; that is, these transitions take place independently of the neighborhood state. The rules can be written as follows:

https://doi.org/10.25088/ComplexSystems.26.4.295

$$s^{t+1} = \begin{cases} \oplus, & \text{if} \sigma_s^t > 0 \\ \ominus, & \text{if} s^t = \oplus \\ \circ, & \text{otherwise} \end{cases}, \quad \mathcal{A}_0 \qquad s^{t+1} = \begin{cases} \oplus, & \text{if} \sigma_s^t = 1 \\ \ominus, & \text{if} s^t = \oplus \\ \circ, & \text{otherwise.} \end{cases} \quad \mathcal{A}_1$$

At the beginning of each computational experiment, the F-actin automaton $\mathcal{A}$ is in a resting state; every node is assigned state $\circ$. An excitation dynamic is initiated by assigning a portion of randomly selected nodes nonresting states: $\oplus$ or $\ominus$. Three stimulation scenarios are considered:

- Single node stimulation: a single node is selected at random and this node is assigned excited state $\oplus$.
- (+)-stimulation: a specified ratio of nodes is selected at random and the selected nodes are assigned excited state $\oplus$.
- (+-)-stimulation: a specified ratio of nodes is selected at random and the selected nodes are assigned either excited state $\oplus$ or refractory state $\ominus$ at random.

The automaton $\mathcal{A}$ is deterministic; therefore, from any initial configuration the automaton evolves into a limit cycle in its state space (where its configuration is repeated after a finite number of steps) or an absorbing state (this is limit cycle length one). For the rules selected, there is only one absorbing state—all nodes are in the resting state. A limit cycle is comprised of configurations where compact patterns of excitation travel along closed paths. A transient period is an interval of automaton evolution from initial configuration to entering a limit cycle or an absorbing state.

For modeling, visualization and analyses we used Processing (www.processing.org), R (www.r-project.org), iGraph (igraph.org) and Chimera (www.cgl.ucsf.edu/chimera).

3. Dynamics of $\mathcal{A}_0$

3.1 Single-Node Stimulation

The excitation propagates as a localized pattern (Figure 2(a–f)). The number of nodes excited at every single step of time varies between one and five (Figure 3(a)). Sometimes an excitation pattern splits into two localizations that travel along their independent pathways. The automaton $\mathcal{A}_0$ always evolves into the absorbing state where all nodes are resting. This is because traveling localizations either cancel each other when they collide or reach cul-de-sacs of their pathways. A distribution of transition periods is shown in Figure 3(b). The mean

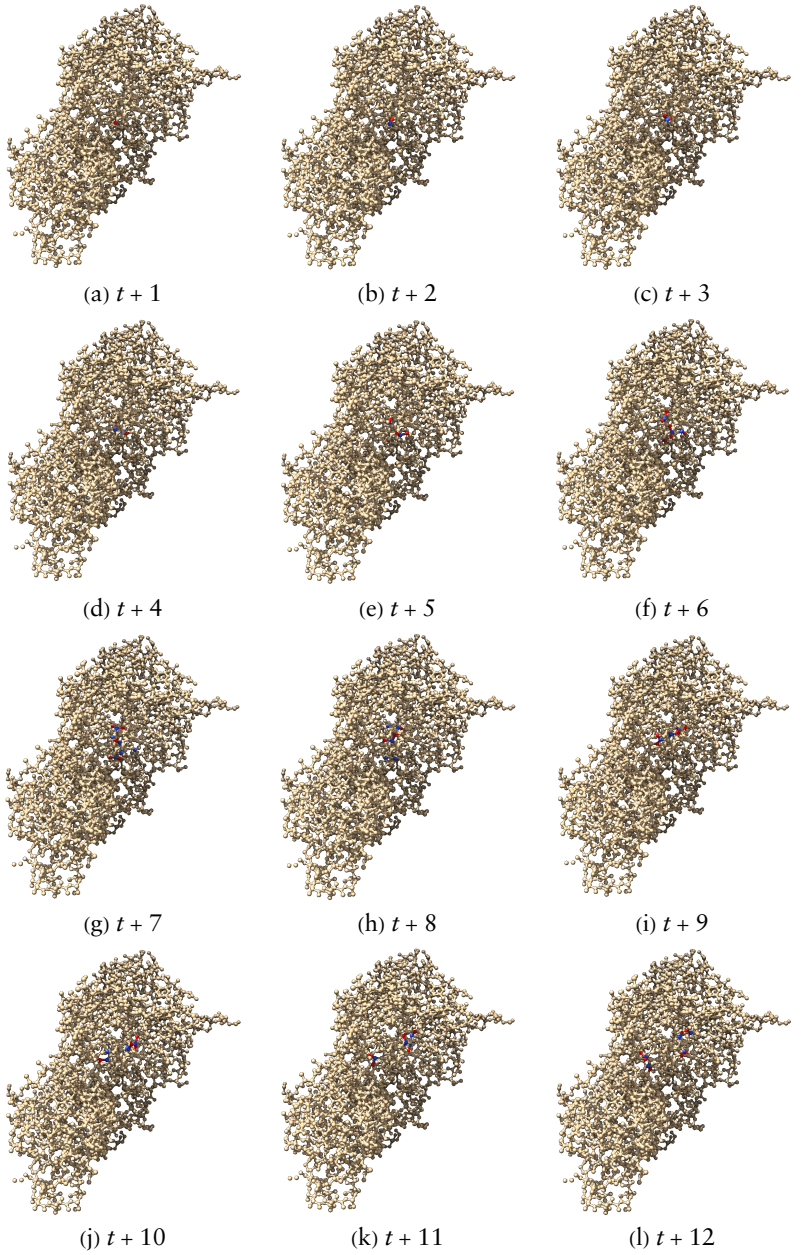

Figure 2. Exemplar excitation dynamics of $\mathcal{A}_0$ in a scenario of single-node stimulation. In the initial configuration, all nodes are resting, but one node is excited. (a–f) Snapshots of the simulation. Excited nodes are red; refractory nodes are blue; resting nodes are light gray.

https://doi.org/10.25088/ComplexSystems.26.4.295

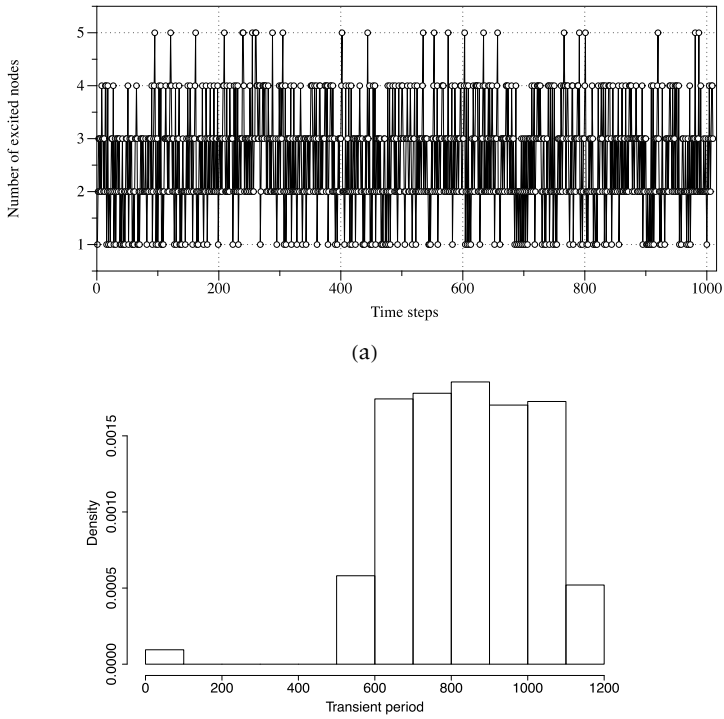

Figure 3. Integral dynamics of rule $\mathcal{A}_0$ automata in scenarios of single-node stimulation. (a) Number of excited nodes at each step of simulation in a single experiment. (b) Distribution of transient periods.

transition period is 840 time steps, the median is 847, the minimum is 2 and the maximum is 1131. Only 29 nodes, when stimulated, lead to excitation development with a transition period between 2 and 15 steps. Stimulation of all 2932 others triggers excitation dynamics for at least 568 steps. The longest transition period is observed when the localized excitation runs along a longest shortest path where the initially stimulated node is a source. The path of the longest excitation is visualized in Figure 4(a). The path matches the backbone of the actin unit (Figure 4(b)).

3.2 (+)-Stimulation

When we stimulate more than one node, the automaton $\mathcal{A}_0$ exhibits several "epicenters" of excitation: the patterns of excitation propagate away from their origins (Figure 5) and populate the graph. This stage is manifested in an increasing number of excited states at each

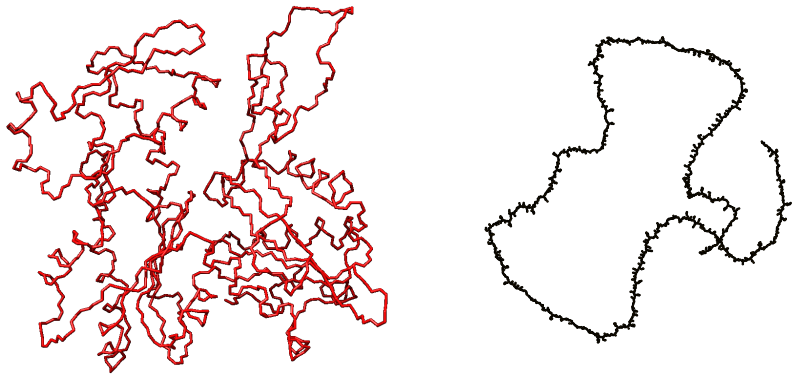

(a) (b)

Figure 4. (a) Longest path of excitation propagation in $\mathcal{A}_0$ displayed by bonds. (b) Actin graph plotted in Kamada–Kawai layout [26] with nodes of degree 1 removed.

step of the evolution (Figure 6(a)). Eventually, depending on distances between sources of excitation, the graph becomes overpopulated with waves and localizations; for example, in Figure 6(a) a peak is reached in seven to eight steps. Then patterns of excitation start colliding with each other and annihilate in the results of the collisions. The number of excited nodes decreases over time (Figure 6(a)), and the graph returns to the totally resting state. The larger the portion of initially excited nodes, the more quickly evolution halts in the resting state (Figure 6(b)). The "more quickly" can be quantified by a polynomial function $p = 4.7 \cdot \rho^{-0.6}$, where p is the length of a transient period and ρ is the ratio of initially excited nodes.

https://doi.org/10.25088/ComplexSystems.26.4.295

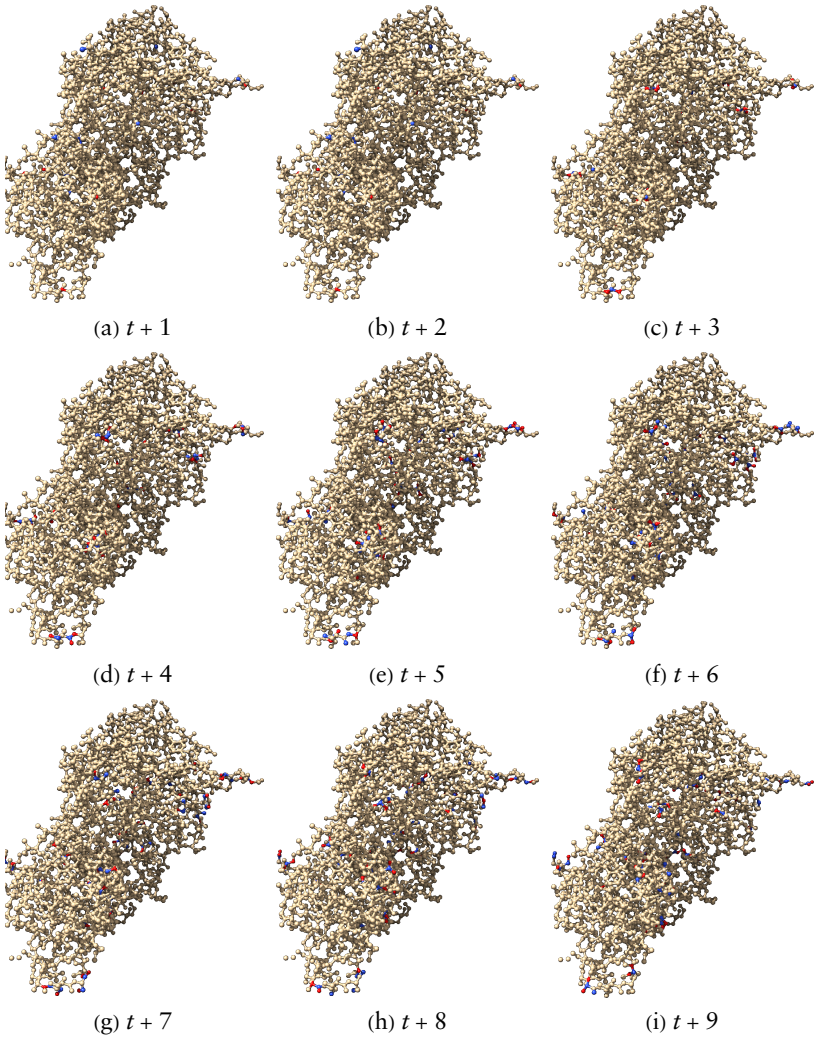

Figure 5. Exemplar dynamics of $\mathcal{A}_1$. In the initially resting configuration, 1% of nodes are excited. Snapshots of the simulation. Edges of $\mathcal{A}$ are shown by gray color, excited nodes are red and refractory nodes are blue; resting nodes are not shown.

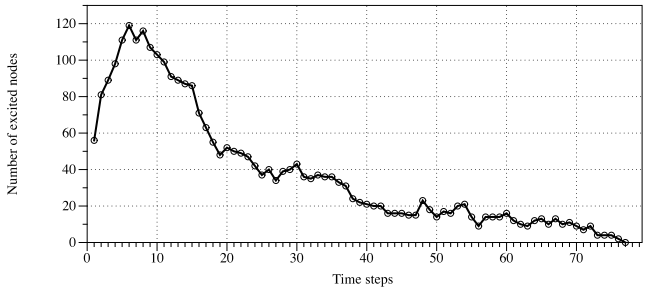

(a)

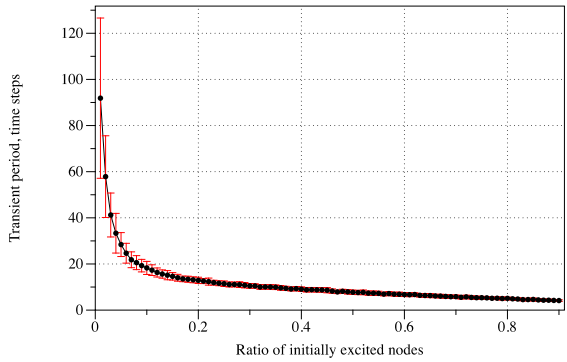

(b)

Figure 6. Integral dynamics of $\mathcal{A}_0$ in scenarios when a portion of nodes are excited initially. (a) The number of excited nodes versus time: initially, 1% of nodes are assigned excited states. (b) Ratio of initially excited nodes versus average transient period. Standard deviation is shown as error bars.

3.3 (+-)-Stimulation

In a "classical" two-dimensional discrete excitable medium, stimulation of the medium with an excited node neighboring with a refractory node leads to formation of a spiral wave. Due to the spiral waves, excitation can persist in a modeled medium indefinitely. F-actin automata follow this principle. When we stimulate nodes of $\mathcal{A}_0$ such that some of the nodes get excited states and some get refractory states, we unleash the excitation patterns. The average level of excitation over trials is proportional to the number of nodes stimulated (see row e in Table 1(a)). The automaton enters a limit cycle (Figure 7). The limit cycle's length varies from 5 to 14 time steps (see row c in Table 1(a)). Apparently, the automaton falls into the longest limit cycles when nearly half of the nodes are stimulated; however, due to high deviation of the results (see row $\sigma(c)$ in Table 1(a)), we

would not state this as a fact. Lengths of transient periods, from stimulation to entering the limit cycle, are over half of the number of nodes in $\mathcal{A}$.

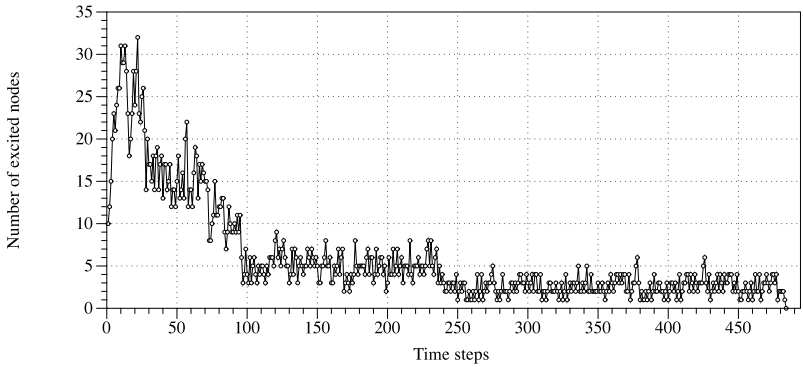

Figure 7. Integral dynamics of $\mathcal{A}_0$ in scenarios when 1% of nodes are assigned excited or refractory states initially.

ρ	p	c	e	$\sigma(p)$	$\sigma(c)$	$\sigma(e)$
10	1613	6	535	1820	1	55
20	1432	5	562	988	0	52
30	1984	7	626	1275	8	108
40	2536	14	598	3064	15	15
50	1583	13	786	610	8	206
60	2614	14	719	3322	14	191
70	2052	9	805	2236	4	207
80	1311	5	705	521	1	180

(a) $\mathcal{A}_0$, (+-)-start.

ρ	p	c	e	$\sigma(p)$	$\sigma(c)$	$\sigma(e)$
0.1	1154	13	570	1251	12	39
0.2	1388	13	553	961	12	50
0.3	893	11	575	362	10	8
0.4	920	24	590	487	11	51
0.5	996	16	575	832	13	11
0.6	746	16	594	238	12	24
0.7	891	16	625	455	11	77
0.8	1354	16	639	408	12	109
0.9	1729	15	577	1368	13	13

(b) $\mathcal{A}_1$, (+)-start.

ρ	p	c	e	$\sigma(p)$	$\sigma(c)$	$\sigma(e)$
0.1	893	118	496	934	355	172
0.2	2328	5	583	1525	0	6
0.3	1953	13	599	1791	12	16
0.4	1957	8	591	2400	8	5
0.5	1785	14	636	2567	12	130
0.6	976	6	706	345	3	179
0.7	1342	11	709	464	13	175
0.8	1170	13	625	620	14	109
0.9	2599	5	593	2452	1	14

(c) $\mathcal{A}_1$, (+-)-start.

	$\mathcal{A}_0$	$\mathcal{A}_1$		
	(+)-start	(+-)-start	(+)-start	(+-)-start
p	840	1997	1118	1667
c	1	10	15	21
e	0	665	588	615

(d) Characteristics averaged.

Table 1. Characterization of excitation dynamics in actin automata $\mathcal{A}$. Dependence of the dynamic on ratios of stimulated nodes. (a) $\mathcal{A}_0$, initially excited ratio ρ of nodes. (b) $\mathcal{A}_1$, initially excited ratio ρ of nodes. (c) $\mathcal{A}_1$, initial ratio ρ of nodes assigned excited and refractory states at random. Data is collected in 10 experiments for each value of ρ. For 10 ratios ρ of initially stimulated nodes, $\rho = 0.1, 0.2, \ldots, 0.9$, we calculated lengths of transient period p, lengths of cycles c, numbers e of excited nodes in a cycle and their standard deviations $\sigma(p)$, $\sigma(c)$, $\sigma(e)$. Values are rounded to integer. (d) Characteristics averaged over all stimulation ratios for each rule and stimulation scenario.

4. Dynamics of $\mathcal{A}_1$

4.1 Single-Node Stimulation

When a single node is excited initially, the automaton $\mathcal{A}_1$ always evolves to a globally resting state. In sampling 70 trials, we found that the average length of the transient period is 862 time steps (standard deviation 230) and the average length of the media transition period is 869. The average transient period to the resting state is 22 steps longer than the one in the automaton $\mathcal{A}_0$.

4.2 (+)-Stimulation

In contrast to automaton $\mathcal{A}_0$, automaton $\mathcal{A}_1$ does not show a pronounced sensitivity to a ratio ρ of initially excited nodes. Transition periods for all values of ρ are grouped around 1112 (Table 1(b)). The automata always evolve to limit cycles. Cycle lengths are around 15

https://doi.org/10.25088/ComplexSystems.26.4.295

time steps, with an excitation level (number of excited nodes) of just below 600 nodes. The system shows a high degree of variability in lengths of transition periods and cycles, as manifested in large values of standard deviations $\sigma(p)$ and $\sigma(c)$. Level of excitation typically remains preserved.

4.3 (+-)-Stimulation

$\mathcal{A}_1$ behaves similarly to the scenario of (+)-start: there are many traveling localizations, which collide and, mostly, annihilate each other. A few localizations survive by finding a cyclic path to travel: if no other localization enters their path, the remaining localizations can cycle "forever." The surviving localizations are responsible for $\mathcal{A}_1$ falling into the limit cycle. An automaton starting with a mix of randomly excited and refractory states usually travels one-and-half times longer to its limit cycle than the same automaton starting only with randomly excited states (compare Table 1(b) and Table 1(c)).

5. Stability of the Dynamics

How does repeated stimulation affect the excitation dynamics of $\mathcal{A}_0$ and $\mathcal{A}_1$? (+)-stimulation of $\mathcal{A}_0$ at any stage of its evolution raises the level of excitation by an amount equivalent to that of a stimulated resting automaton (Figure 8). Thus repeated stimulation prolongs return of the automaton to its resting state. In the scenario of (+-)-stimulation, $\mathcal{A}_0$ evolves to a limit cycle. Repeated (+-)-stimulation of the automaton while it is in the limit cycle causes the automaton to change its trajectory in a state space. This change is characterized by an initially reduced level of excitation. Typically, the excitation level drops by 100 to 150 nodes at the moment of stimulation. The level of excitation returns to its "pre-stimulation" value in 400 to 500 time steps.

6. Implementation of Memory

F-actin automata entering limit cycles could act as models of information storage in actin filaments. The minimal length of a limit cycle detected is five time steps. Thus aromatic rings could be a substrate responsible for some patterns of cycling excitation dynamics. Let an aromatic ring automaton be stimulated such that a node is assigned an excited state and one of its neighbors is assigned a refractory state. The wave of excitation (comprised of one excited and one refractory state) propagates into the direction of its excited head (Figure 10(a)).

The excitation running along the aromatic ring cannot be extinguished by stimulation of one resting node (Figure 10(b–e)) or two resting nodes (Figure 10(f–h)). This is because an excited node surrounded by two resting neighbors excites both resting neighbors. Thus excitation waves propagate along the ring in both directions. Therefore, even if the original excitation wave is canceled by external stimulation, then a similar running wave will emerge. To extinguish the excitation in the aromatic ring, we must externally excite all four resting nodes or force them into a refractory state.

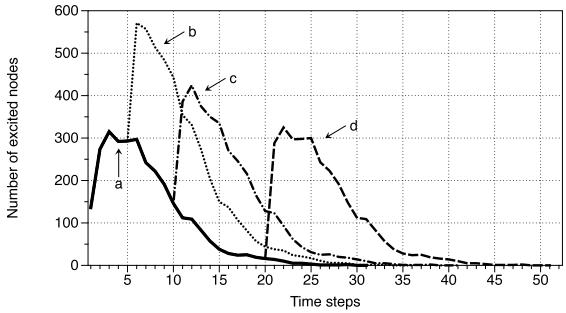

Figure 8. Dynamics of $\mathcal{A}_0$ automaton under repeated stimulation. In each trial, 5% of nodes were initially excited. (a) No more stimulation applied. (b–d) Automaton was stimulated by exciting 5% of nodes at the fifth step (b), tenth step (c) and twentieth step. (d) Steps of evolution.

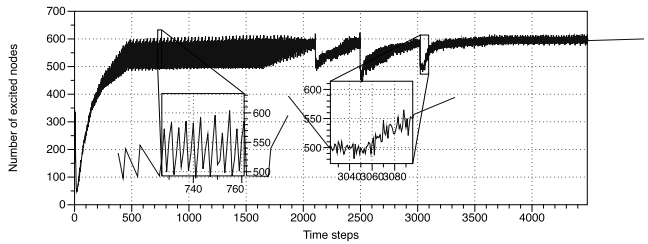

Figure 9. Dynamics of $\mathcal{A}_0$ automaton under repeated stimulation. Initially, 10% of nodes were assigned an excited or refractory state at random. When the automaton reached the limit cycle, the stimulation was repeated.

https://doi.org/10.25088/ComplexSystems.26.4.295

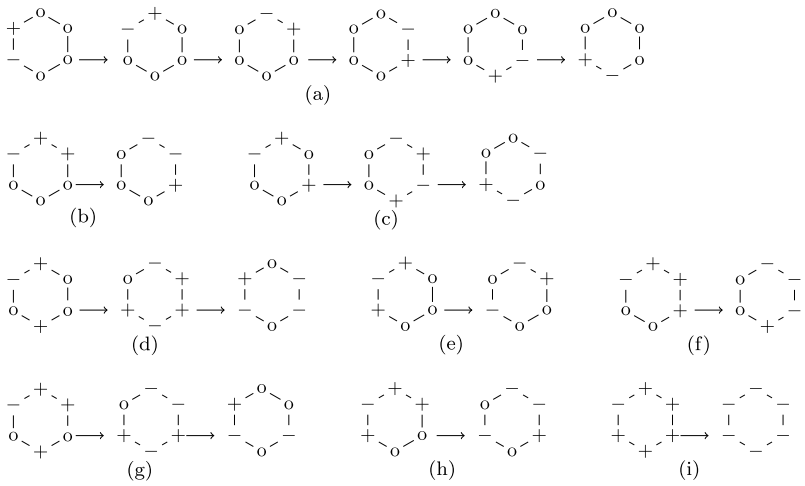

Figure 10. Excitation dynamics of aromatic ring automaton governed by $\mathcal{A}_0$. (a) Propagation of excitation wave on undisturbed ring automaton. (b–i) Stimulation of ring automaton.

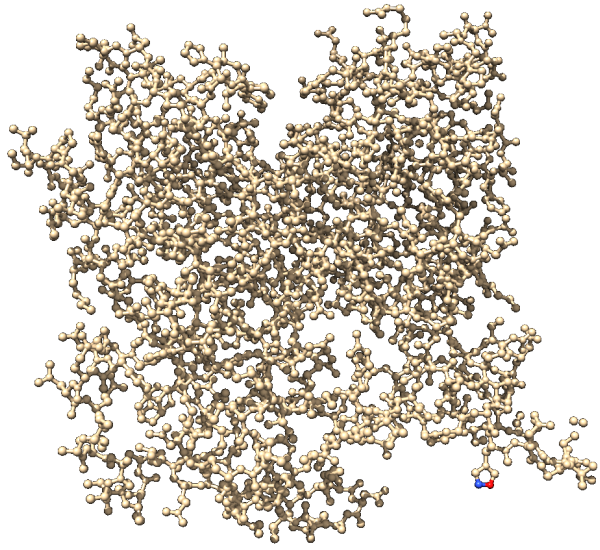

Figure 11. Configuration of resting $\mathcal{A}_0$ at the moment of external stimulation of histidine's aromatic ring. Resting nodes are light gray; excited nodes are red; refractory nodes are blue.

The excited aromatic rings act as generators of excitation in F-actin automata. Let us consider an example. In Figure 11, we see histidine's aromatic ring stimulated: one node is assigned an excited state and its

neighbor a refractory state. The wave of excitation travels along the ring clockwise (Figure 12(a–c)). When excitation reaches a node linked to the rest of the graph, the excitation propagates along the "bridge" (Figure 12(d)). The excitation then propagates further inside the graph (Figure 12(e–f)), splitting into two compact excitation patterns at the junctions (Figure 12(g–h)). The overall pattern of excitation in $\mathcal{A}_0$ recorded at the ninetieth step of evolution is shown in Figure 13.

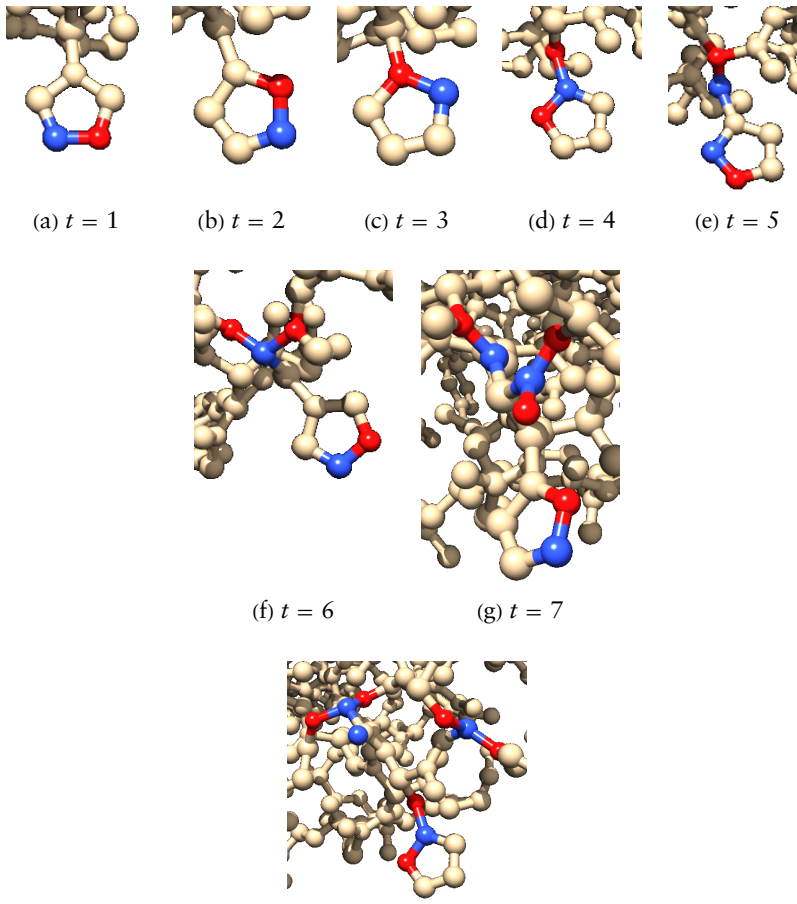

Figure 12. Excitation dynamics of $\mathcal{A}_0$ triggered by excitation of histidine's aromatic ring. The first 10 steps of the automaton evolution are shown. Only part of the graph adjacent to excitation is displayed. Resting nodes are light gray; excited nodes are red; refractory nodes are blue.

https://doi.org/10.25088/ComplexSystems.26.4.295

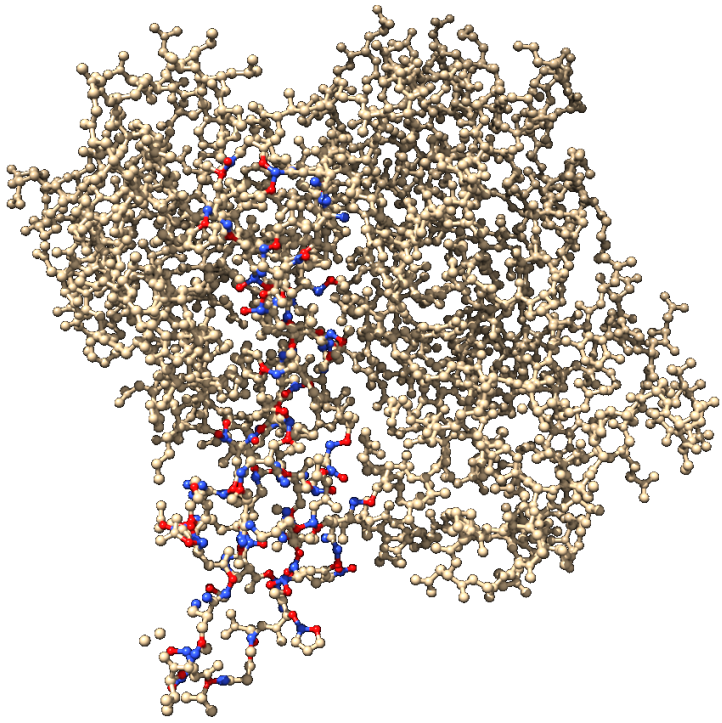

Figure 13. Pattern of excitation of $\mathcal{A}_0$ triggered by excitation of histidine's aromatic ring as shown in Figure 12. The pattern is recorded at the ninetieth step of evolution. Resting nodes are light gray; excited nodes are red; refractory nodes are blue.

7. Logical Gates

We search for the Boolean logical gates by selecting a pair of nodes, exciting these nodes by representing all possible combinations of inputs, and checking the states of all other nodes in the automaton. Let two nodes i and j be selected as inputs and one node p as an output. Boolean logical variables are x and y (inputs) and z (output). Automaton $\mathcal{A}$ is in a resting state. Logical values of inputs are converted to initial states of input nodes as follows. If $x = \text{TRUE}$ then $s_i^0 = \oplus$; if $y = \text{TRUE}$ then $s_j^0 = \oplus$. We allow the automaton to evolve until a limit cycle or an absorbing state is reached. During the automaton's evolution, we monitor the state of the output node p. If at some time step t we have $s_p^t = \oplus$, we assign $z = \text{TRUE}$.

We sampled 100 pairs of input nodes, selected at random. For each pair, we tested outputs on each of 2961 nodes (in many cases, several nodes can act as outputs for the same input pair). Statistics are shown

in Table 2. Almost every pair of nodes tested can act as input of one of the logical gates. Both automata $\mathcal{A}_0$ and $\mathcal{A}_1$ implement gates OR ($x + y$) and AND-NOT ($x\bar{y}$ and $\bar{x}y$) with similar frequencies. Automaton $\mathcal{A}_1$ also implements gate XOR ($\bar{x}y + x\bar{y}$), albeit there are only two potential outputs for each input pair on average. Exemplar locations of input and output nodes in an XOR gate are shown in Figure 14. Frequencies of potential output nodes vary between the gates. Almost every node can be an output for an XOR gate. Only 36–39 nodes are found to be outputs for an AND-NOT gate, and just two nodes can be outputs for an XOR gate (Table 2).

	$x\bar{y}$	$\bar{x}y$	$x + y$	$\bar{x}y + x\bar{y}$
$\mathcal{A}_0$				
n	97	97	97	0
m ($\sigma(m)$)	38 (10)	39 (10)	2854 (12)	0
$\mathcal{A}_1$				
n	95	95	97	50
m ($\sigma(m)$)	36 (7)	39 (8)	2802 (111)	2 (1)

Table 2. Data on gates discovered in F-actin automata $\mathcal{A}_0$ and $\mathcal{A}_1$. n is the number of input node pairs discovered in 100 trials, m is the number of output nodes (that show the same outputs) for each discovered gate, and $\sigma(m)$ is its standard deviation.

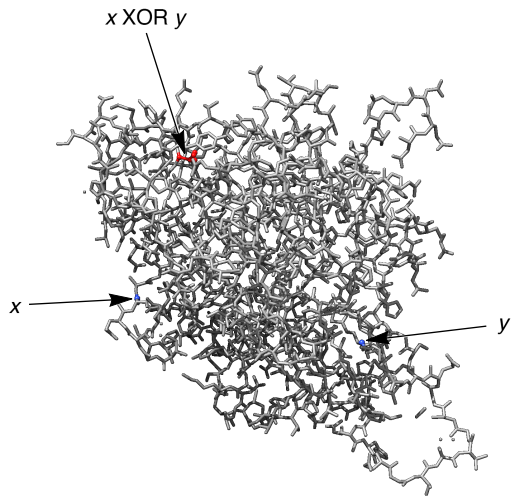

Figure 14. XOR gate architecture. Input nodes i and j are blue; output nodes (each one of the nodes reports $x \oplus y$) are red.

https://doi.org/10.25088/ComplexSystems.26.4.295

8. Discussion

A concept of molecular automata is neither novel nor rigorously defined. Work has been done on automaton genotype-phenotype state-transition functions [27], cellular automaton models of molecular arrays [28, 29], enzymatic networks [30, 31], quantum-dot cellular automata applied to molecular topologies [32, 33], molecular-sized switches [31, 34] and self-assembling molecular automata [35]. Most of the results implement automata at the super-molecular level. Soliton automata [36, 37] are the finest and oldest example of the submolecular automata: they employ flip-flop operations of switching between single and double bonds; this is somewhat reminiscent of structurally dynamic cellular automata [38]. We presented submolecular automata, where every atom is a finite-state machine (automaton) and chemical bonds are links between the automata.

An automaton model of an F-actin unit is a fast prototyping tool for studying the dynamics of excitation, voltage solitons and traveling localizations in actin filaments, allowing for controlling propagation of localizations at the atomic level. Two rules of excitation were analyzed. The first rule states that a resting node excites if it has at least one excited neighbor ($\mathcal{A}_0$): this is a classical threshold excitation rule. The second rule states that a resting node excites if it has exactly one excited neighbor ($\mathcal{A}_1$): this may be seen as a rule of nonlinear excitation, because only a narrow band of local excitation triggers excitation in the node. We did not consider other ranges of thresholds or excitation intervals, because they always lead to extinction of excitation at the very beginning of the evolution. Both rules support propagating excitations. Automata $\mathcal{A}_0$ show longer transition periods, smaller limit cycles and larger average levels of excitation than automata $\mathcal{A}_1$ (Table 1(d)). When a resting automaton $\mathcal{A}_0$ is stimulated by external excitation of some nodes, the excitation patterns spread all over the automaton graph but then decline and extinguish. Stimulation of actin automata with a mix of excited and refractory states leads to excitation dynamics with longer transient periods and formation of repeated patterns of excitation, analogous to oscillatory structures. The limit cycles are stable: an automaton subjected to repeated stimulation always slides back to its pre-stimulation activity level.

Due to substantial noise tolerance of excitation waves propagating in aromatic rings, the rings could be seen as memory devices in a hypothetical actin computer. Assume an excited aromatic ring represents one bit. To write a bit, we excite one node and inhibit (force into refractory state) one of its neighbors. To erase a bit, we must excite or inhibit all resting nodes. An F-actin unit contains 40 rings

(eight of histidine, 12 of phenylalanine, four of tryptophane and 16 of tyrosine); see configuration of the aromatic rings in Figure 15. Thus an F-actin unit can store 40 bits. The maximum diameter of an actin filament is 8 nm [39, 40]. An actin filament is composed of overlapping units of F-actin (Figure 1(a)). Thus, the diameter of a single unit is about 4 nm. This gives us an estimate for a density of bits stored in ensembles of F-actin units: 64 petabits per square inch ($6.452 \cdot 10^{16}$ per square inch). Such memory density substantially exceeds not only the areal density 2.2 gigabits of a compact disc but even the latest areal density of 2.77 terabits per square inch revealed by Micron [41]. Density of gates AND-NOT, measured by a number of potential output nodes, is almost the same as density of bit-storage units; density of XOR gates is 20 times less.

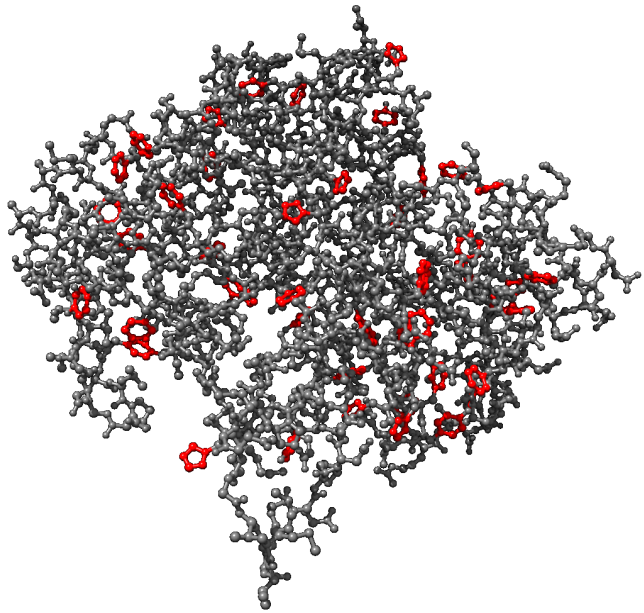

Figure 15. F-actin molecule with aromatic rings highlighted in red.

The XOR gate is a rare species not only in automaton models of the F-actin molecule but in many other natural systems. The frequencies of a gate's occurrences in a material might act as a measure of the gate's complexity. Let gates g_1 and g_2 be discovered with frequencies $f(g_1)$ and $f(g_2)$; we say gate g_1 is easier to develop or evolve than gate g_2: $g_1 g_2$ if $f(g_1) > f(g_2)$. The hierarchies of gates obtained using evolutionary techniques in liquid crystals [42], light-sensitive modification

https://doi.org/10.25088/ComplexSystems.26.4.295

of the Belousov–Zhabotinsky system [43], morphological complexity of one-dimensional cellular automata governed by the gate [44] and gates generated in slime mold *Physarum polycephalum* [45] are compared with the hierarchies of gates found in F-actin automata $\mathcal{A}_0$ and $\mathcal{A}_1$ below:

- Gates in F-actin automaton $\mathcal{A}_0$: OR ▷ AND-NOT.
- Gates in F-actin automaton $\mathcal{A}_1$: OR ▷ AND-NOT ▷ XOR.
- Gates in liquid crystals [42]: {OR, NOR} ▷ AND ▷ NOT ▷ NAND ▷ XOR.
- Gates in Belousov–Zhabotinsy medium [43]: AND ▷ NAND ▷ XOR.
- Gates in cellular automata [44]: OR ▷ NOR ▷ AND ▷ NAND ▷ XOR.
- Gates in *Physarum* [45]: AND ▷ OR ▷ NAND ▷ NOR ▷ XOR ▷ XNOR.

F-actin follows a general trend: gate AND is easier to find than gate OR, and gate OR is easier to find than gate XOR. The gate XNOR is the rarest gate, and it could not be found in principle in F-actin automata because there is no self-excitation: two resting inputs cannot make an excited output.

References

[1] F. B. Straub, "Actin, II," in *Muscular Contraction, Blood Coagulation* (A. Szent-Gyorgyi, ed.), Studies from the Institute of Medical Chemistry University Szeged, Vol. III, Basel, New York: S. Karger, 1943 pp. 23–37.

[2] E. D. Korn, "Actin Polymerization and Its Regulation by Proteins from Nonmuscle Cells," *Physiological Reviews*, **62**(2), 1982 pp. 672–737.

[3] A. G. Szent-Györgyi, "The Early History of the Biochemistry of Muscle Contraction," *The Journal of General Physiology*, **123**(6), 2004 pp. 631–641. doi:10.1085/jgp.200409091.

[4] T. Oda, M. Iwasa, T. Aihara, Y. Maéda and A. Narita, "The Nature of the Globular- to Fibrous-Actin Transition," *Nature*, **457**(7228), 2009 pp. 441–445. doi:10.1038/nature07685.

[5] G. M. Cooper and R. E. Hausman, *The Cell: A Molecular Approach*, 3rd ed., Washington, DC: ASM Press; Sunderland, MA: Sinauer Associates, 2004.

[6] L. A. Cingolani and Y. Goda, "Actin in Action: The Interplay between the Actin Cytoskeleton and Synaptic Efficacy," *Nature Reviews Neuroscience*, **9**(5), 2008 pp. 344–356. doi:10.1038/nrn2373.

[7] S. R. Hameroff, "Coherence in the Cytoskeleton: Implications for Biological Information Processing," in *Biological Coherence and Response to External Stimuli* (H. Fröhlich, ed.), Berlin, Heidelberg: Springer, 1988 pp. 242–265.

[8] S. Rasmussen, H. Karampurwala, R. Vaidyanath, K. S. Jensen and S. Hameroff, "Computational Connectionism within Neurons: A Model of Cytoskeletal Automata Subserving Neural Networks," *Physica D: Nonlinear Phenomena*, **42**(1–3), 1990 pp. 428–449. doi:10.1016/0167-2789(90)90093-5.

[9] B. Ludin and A. Matus, "The Neuronal Cytoskeleton and Its Role in Axonal and Dendritic Plasticity," *Hippocampus*, **3**(S1), 1993 pp. 61–71.

[10] M. Conrad, "Cross-Scale Information Processing in Evolution, Development and Intelligence," *BioSystems*, **38**(2–3), 1996 pp. 97–109. doi:10.1016/0303-2647(95)01579-5.

[11] J. A. Tuszynski, J. A. Brown and P. Hawrylak, "Dielectric Polarization, Electrical Conduction, Information Processing and Quantum Computation in Microtubules: Are They Plausible?," *Philosophical Transactions of the Royal Society A. Mathematical, Physical and Engineering Sciences*, **356**(1743), 1998 pp. 1897–1926. doi:10.1098/rsta.1998.0255.

[12] A. Priel, J. A. Tuszynski and H. F. Cantiello, "The Dendritic Cytoskeleton as a Computational Device: An Hypothesis," in *The Emerging Physics of Consciousness* (J. A. Tuszynski, ed.), Berlin, Heidelberg: Springer, 2006 pp. 293–325.

[13] D. Debanne, "Information Processing in the Axon," *Nature Reviews Neuroscience*, **5**(4), 2004 pp. 304–316. doi:10.1038/nrn1397.

[14] A. Priel, J. A. Tuszynski and N. J. Woolf, "Neural Cytoskeleton Capabilities for Learning and Memory," *Journal of Biological Physics*, **36**(3), 2010 pp. 3–21. doi:10.1007/s10867-009-9153-0.

[15] L. Jaeken, "A New List of Functions of the Cytoskeleton," *IUBMB Life*, **59**(3), 2007 pp. 127–133. doi:10.1080/15216540701320593.

[16] E. Fifková and R. J. Delay, "Cytoplasmic Actin in Neuronal Processes as a Possible Mediator of Synaptic Plasticity," *The Journal of Cell Biology*, **95**(1), 1982 pp. 345–350. doi:10.1083/jcb.95.1.345.

[17] C.-H. Kim and J. E. Lisman, "A Role of Actin Filament in Synaptic Transmission and Long-Term Potentiation," *The Journal of Neuroscience*, **19**(11), 1999 pp. 4314–4324.

[18] C. Dillon and Y. Goda, "The Actin Cytoskeleton: Integrating Form and Function at the Synapse," *Annual Review of Neuroscience*, **28**(1), 2005 pp. 25–55. doi:10.1146/annurev.neuro.28.061604.135757.

[19] A. Adamatzky and R. Mayne, "Actin Automata: Phenomenology and Localizations," *International Journal of Bifurcation and Chaos*, **25**(2), 2015 1550030. doi:10.1142/S0218127415500303.

[20] J. A. Tuszynski, S. Portet, J. M. Dixon, C. Luxford and H. F. Cantiello, "Ionic Wave Propagation along Actin Filaments," *Biophysical Journal*, **86**(4), 2004 pp. 1890–1903. doi:10.1016/S0006-3495(04)74255-1.

[21] S. Siccardi and A. Adamatzky, "Actin Quantum Automata: Communication and Computation in Molecular Networks," *Nano Communication Networks*, **6**(1), 2015 pp. 15–27. doi:10.1016/j.nancom.2015.01.002.

[22] S. Siccardi, J. A. Tuszynski and A. Adamatzky, "Boolean Gates on Actin Filaments," *Physics Letters A*, **380**(1–2), 2016 pp. 88–97. doi:10.1016/j.physleta.2015.09.024.

[23] S. Siccardi and A. Adamatzky, "Quantum Actin Automata and Three-Valued Logics," *IEEE Journal on Emerging and Selected Topics in Circuits and Systems*, **6**(1), 2016 pp. 53–61. doi:10.1109/JETCAS.2016.2528722.

[24] S. Siccardi and A. Adamatzky, "Logical Gates Implemented by Solitons at the Junctions between One-Dimensional Lattices," *International Journal of Bifurcation and Chaos*, **26**(6), 2016 1650107. doi:10.1142/S0218127416501078.

[25] S. Siccardi and A. Adamatzky, "Models of Computing on Actin Filaments," in *Advances in Unconventional Computing* (A. Adamatzky, ed.), New York: Springer, 2016 pp. 309–346.

[26] T. Kamada and S. Kawai, "An Algorithm for Drawing General Undirected Graphs," *Information Processing Letters*, **31**(1), 1989 pp. 7–15. doi:10.1016/0020-0190(89)90102-6.

[27] M. Conrad, "Molecular Automata," in *Physics and Mathematics of the Nervous System* (M. Conrad, W. Güttinger and M. Dal Cin, eds.), Berlin, Heidelberg: Springer-Verlag, 1974 pp. 419–430.

[28] S. R. Hameroff, J. E. Dayhoff, R. Lahoz-Beltra, A. V. Samsonovich and S. Rasmussen, "Models for Molecular Computation: Conformational Automata in the Cytoskeleton," *Computer*, **25**(11), 1992 pp. 30–39. doi:10.1109/2.166406.

[29] T. Nozawa and T. Kondo, "Construction of Reversible Lattice Molecular Automata," *International Journal of Modern Physics C*, **20**(6), 2009 pp. 901–929. doi:10.1142/S0129183109014072.

[30] P. C. Marijuán and J. Westley, "Enzymes as Molecular Automata: A Reflection on Some Numerical and Philosophical Aspects of the Hypothesis," *Biosystems*, **27**(2), 1992 pp. 97–113. doi:10.1016/0303-2647(92)90050-9.

[31] E. Katz, "Molecular Information Processing: From Chemical to Biochemical Systems—From Molecular Computers and Automata to Digital Biosensors and Actuators," *Israel Journal of Chemistry*, **51**(1), 2011 pp. 13–14. doi:10.1002/ijch.201000075.

[32] C. S. Lent, B. Isaksen and M. Lieberman, "Molecular Quantum-Dot Cellular Automata," *Journal of the American Chemical Society*, **125**(4), 2003 pp. 1056–1063. doi:10.1021/ja026856g.

[33] Y. Lu, M. Liu and C. Lent, "Molecular Quantum-Dot Cellular Automata: From Molecular Structure to Circuit Dynamics," *Journal of Applied Physics*, **102**(3), 2007 034311. doi:10.1063/1.2767382.

[34] F. L. Carter, "The Molecular Device Computer: Point of Departure for Large Scale Cellular Automata," *Physica D: Nonlinear Phenomena*, **10**(1–2), 1984 pp. 175–194. doi:10.1016/0167-2789(84)90260-4.

[35] G. Terrazas, H. Zenil and N. Krasnogor, "Exploring Programmable Self-Assembly in Non-DNA Based Molecular Computing," *Natural Computing*, **12**(4), 2013 pp. 499–515. doi:10.1007/s11047-013-9397-2.

[36] J. Dassow and H. Jürgensen, "Soliton Automata," in *Proceedings of the International Conference on Fundamentals of Computation Theory (FCT '87)*, London: Springer-Verlag, 1987 pp. 95–102.

[37] J. Dassow and H. Jürgensen, "Soliton Automata," *Journal of Computer and System Sciences*, **40**(2), 1990 pp. 154–181. doi:10.1016/0022-0000(90)90010-I.

[38] A. Ilachinski and P. Halpern, "Structurally Dynamic Cellular Automata," *Complex Systems*, **1**(3), 1987 pp. 503–527. www.complex-systems.com/pdf/01-3-7.pdf.

[39] P. B. Moore, H. E. Huxley and D. J. DeRosier, "Three-Dimensional Reconstruction of F-Actin, Thin Filaments and Decorated Thin Filaments," *Journal of Molecular Biology*, **50**(2), 1970 pp. 279–288. doi:10.1016/0022-2836(70)90192-0.

[40] J. A. Spudich, H. E. Huxley and J. T. Finch, "Regulation of Skeletal Muscle Contraction: II. Structural Studies of the Interaction of the Tropomyosin-Troponin Complex with Actin," *Journal of Molecular Biology*, **72**(3), 1972 pp. 619–620. doi:10.1016/0022-2836(72)90180-5.

[41] L. Mearian, "Flash Memory's Density Surpasses Hard Drives for First Time," *Computerworld*, Feb 8, 2016. www.computerworld.com/article/3030642/data-storage/flash-memorys-density-surpasses-hard-drives-for-first-time.html.

[42] S. Harding and J. F. Miller, "Evolution *in Materio*: Evolving Logic Gates in Liquid Crystal," in *Proceedings of the Workshop on Unconventional Computing at ECAL 2005 VIIIth European*, Beckington, UK, 2005 pp. 133–149.

[43] R. Toth, C. Stone, A. Adamatzky, B. de Lacy Costello and L. Bull, "Dynamic Control and Information Processing in the Belousov–Zhabotinsky Reaction Using a Coevolutionary Algorithm," *The Journal of Chemical Physics*, **129**(18), 2008 184708. doi:10.1063/1.2932252.

[44] A. Adamatzky and L. Bull, "Are Complex Systems Hard to Evolve?," *Complexity*, **14**(6), 2009 pp. 15–20. doi:10.1002/cplx.20269.

[45] S. Harding, J. Koutnik, K. Greff, J. Schmidhuber and A. Adamatzky, "Discovering Boolean Gates in Slime Mould." arxiv.org/abs/1607.02168.